SUPPORTING INFORMATION

Two dimensional dipolar coupling in monolayers of silver and gold nanoparticles on a dielectric substrate

*Yu Liu, Sylvie Begin-Colin, Benoit P. Pichon, Cedri Leuvrey, Dris Ihiawakrim, Mircea Rastei, Guy Schmerber, Mircea Vomir, Jean Yves Bigot**

Institut de Physique et Chimie des Matériaux de Strasbourg, UMR 7504, CNRS, Université de Strasbourg, 23, rue du Loess, BP43, 67034 Strasbourg, France

E-mail: bigot@unistra.fr

Section 1: Synthesis and characterization of silver and gold nanoparticles

- **Materials**

Gold (III) chloride trihydrate ($HAuCl_4 \cdot 3H_2O$, Aldrich, 99.9$^+$%), silver acetate (Aldrich, 99.99%), oleylamine (Aldrich, technical grade, 70%), 1-dodecanethiol (Aldrich, >=98%), octhyle ether (Sigma, 99%), toluene (Decon Labs, Inc., 99.8%), and chloroform (EMD, ACS Reagent Grade) were used as received without further purification.

a) Synthesis of oleylamine capped Au and Ag Nanoparticles

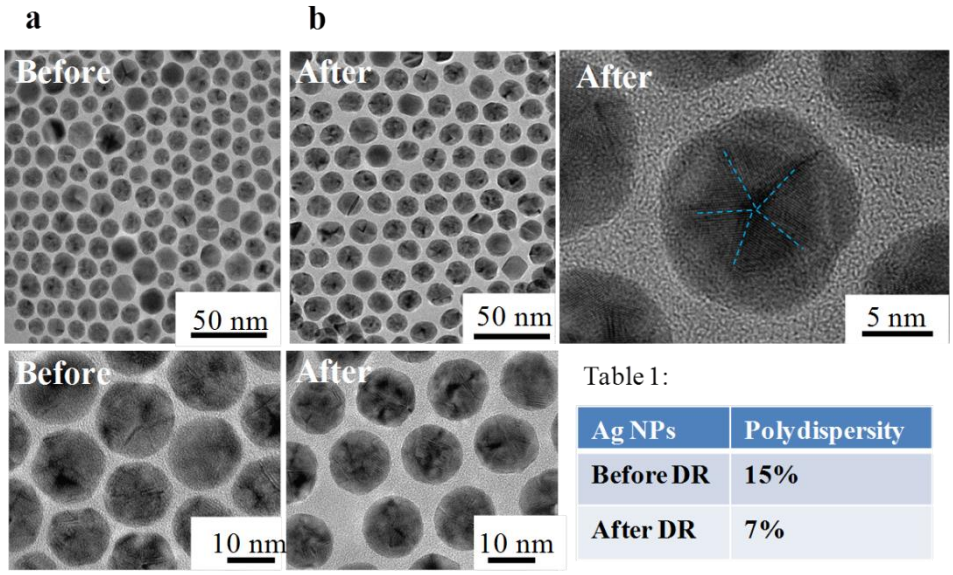

Table 1:

Ag NPs	Polydispersity
Before DR	15%
After DR	7%

Figure S1. Transmission Electron Microscopy images showing the morphology and monodispersity of Ag NPs before (a) and after (b) the digestive ripening step. Right: High magnification TEM image of silver NPs with icosahedral geometry. The table on the right describes the polydispersity percentage obtained from TEM images statistic count.

The amount of oleylamine to the NPs weight ratio was determined by thermogravimetric analysis: 13 wt. % was deduced for Au NPs and 40 wt. % for Ag NPs. We should mention

that, for Ag NPs suspension, two times purification after synthesis by centrifugation leads to aggregation of NPs suspension during the day.

b) Characterization of films

The formation of films was confirmed by scanning electron microscopy (SEM) (Figure 2 in main text). The SEM images showed more defects in Ag LB films than in the Au LB ones. The difficulty in obtaining monodisperse colloidal suspension of Au or Ag NPs with sizes larger than 10 nm in organic solvent has been widely reported[1,2,3] and the size of Ag NPs is slightly larger than that of Au NPs.

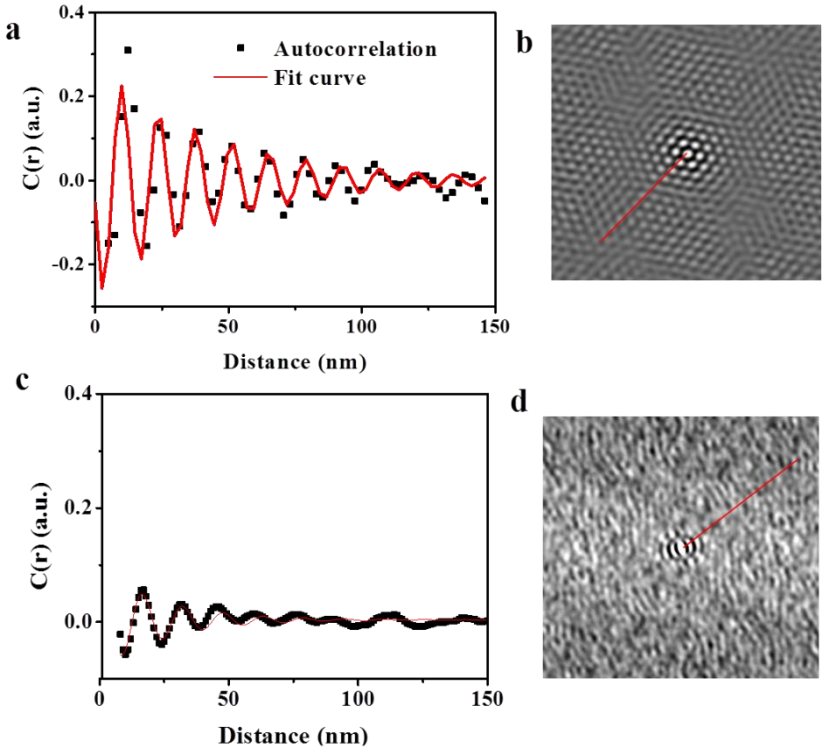

Figure S2. Radial profile of LB monolayer with autocorrelation spectrum (a) extracted along the line in (b) for Au NPs (c) extracted along the line in (d) for Ag NPs. See more details in refs. 4, 5.

The analysis of the AFM profile of the drop casting assemblies of NPs confirms the multilayer character of the sample (Figures S3 b), S3 d)) (the zero corresponds to the substrate surface). The drop casting film may thus be considered as a 3D assembly of NPs and a mean interparticle distance has been determined by considering the interparticle distance observed on TEM grids. Indeed, the LB technique induces a compressing step which promotes closer interparticle distances. This is not the case of drop casting which allows a free organization of NPs in a similar way to what is observed when depositing a drop of suspension to prepare TEM grids. Mean interparticle distances of 1.9 ±1 and 3 ±1 nm were thus determined for

drop-casted Au and Ag films respectively in good agreement with SEM estimations (Table 1 in main text).

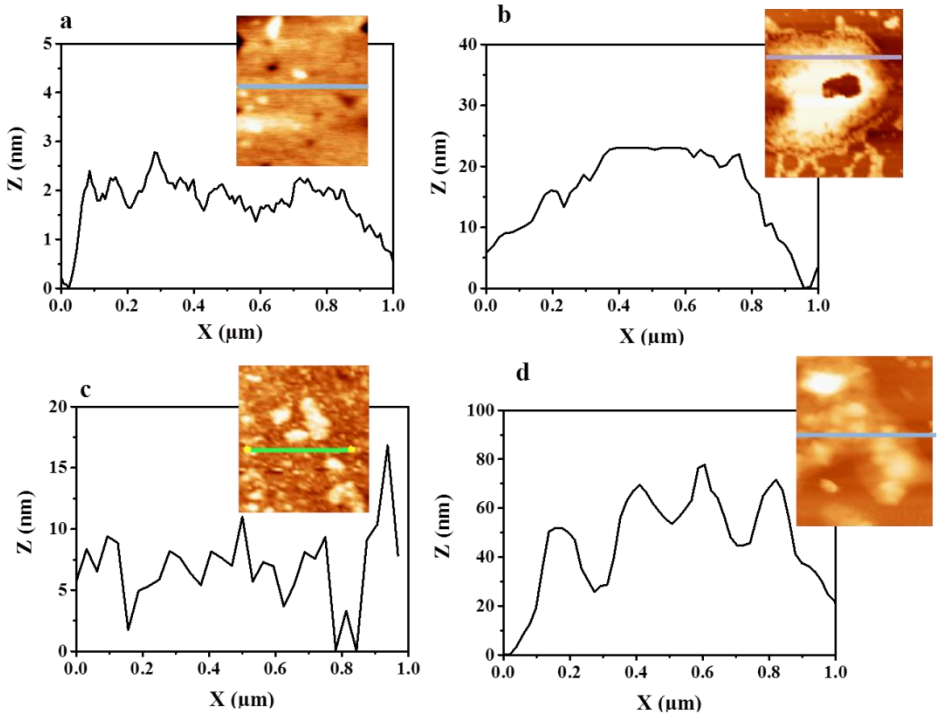

Figure S3. Atomic Force Microscopy profiles on Au and Ag films. Drop casting deposition leads to bilayer or multilayer films as confirmed by AFM profile. a) Au monolayer with a roughness of ~2.2 nm. b) Au NPs bilayer with 25 nm thickness, c) Ag monolayer with ~8 nm roughness. d) Ag NPs multilayers have a thickness in the range 50 to 70 nm.

Section 2. Modeling of the 2D and 3D nanoparticles optical response

a) Bulk dielectric function of Au and Ag

We first model the bulk dielectric functions of Au and Ag that are used to calculate the optical response of the nanoparticles. For this, take into account the intraband and interband transitions usually considered in noble metals.

The intraband part $\tilde{\varepsilon}_f$ of the complex dielectric function $\tilde{\varepsilon}$ corresponds to the Drude Model:

$$\tilde{\varepsilon}_f(\omega) = 1 - \frac{\omega_p^2}{\omega\,(\omega + i\gamma)} \qquad \text{(S1)}$$

Where $\hbar\omega_p$ and $\hbar\gamma$ are the plasmon energy and the damping of free electrons and $\hbar\omega$ the photon energy. The interband part $\tilde{\varepsilon}_{ib}$ is deduced from the Lindhart RPA theory[6], in the case of a two-bands model with one dispersion-less band (d electrons) and a parabolic dispersion for the conduction band (p electrons):

$$\tilde{\varepsilon}_{ib}(\omega) = 2K \int_{E_g}^{\infty} dE \ \frac{\sqrt{E - E_g}}{E} \left[1 - F(E,T)\right] \frac{1}{\left[(\hbar\omega)^2 - E^2 - (\hbar\alpha)^2 - 2i\,\hbar\omega\,\hbar\alpha\right]}$$
$$F(E,T) = \left[1 + \exp\frac{(E - E_F)}{k_B T}\right]^{-1} \qquad \text{(S2)}$$

Where E, $\hbar\alpha$, $k_B T$, E_F *and* E_g are respectively: the interband energy and damping for a given electron, the thermal energy at temperature T, as well the Fermi and band gap energies. $F(E,T)$ is the Fermi distribution which accounts for the Pauli exclusion principle. Note that equation (S2) has to be modified when taking into account the multiple interband transitions like p $\rightarrow$ s as well as the non-parabolicity of the bands in the Brillouin zone. But these details turn out to be minor refinements in the present context. The parameter K contains the detailed microscopic parameters such as the dipole moment of the transition (considered in first approximation to be independent of the k-vector in the Brillouin zone) and the effective mass of the p band.

In the bulk, the damping of free electrons is known to depend on their mean free path, which depends on the electron-phonon interaction and the structural defects. A typical low value is $\hbar\gamma \approx 0.05eV$ for good films. The interband damping constant depends on the electron-electron scattering which for a given temperature T and energy E above the Fermi level E_F can be approximated, according to the Pines and Nozière theory, by[7]:

$$\hbar\alpha = W_{ee} \frac{\left(E - E_F\right)^2 + \left(\pi k_B T\right)^2}{\left[1 + \exp\frac{(E_F - E)}{k_B T}\right]} + \hbar\alpha_0 \qquad \text{(S3)}$$

Where W_{ee} is the electron-electron scattering cross-section. $\hbar\alpha_0$ is an additional constant damping due to structural defects and phonon scattering, or auger processes, particularly for the electrons well above the Fermi energy. It is strongly dependent on the quality of the metallic films. Such approach has been successfully used for modelling the ultrafast dynamics of Cu and Ag nanoparticles[8,9] or for arrays of holes in metallic films[10]. Generally speaking it presents the advantage of taking into account the temperature variation which is not necessary in the present work where only static optical measurements are considered.

With this simple two-band model we have fitted the dielectric functions for Gold and Silver as determined experimentally by Jonhson & Christy[11]. Figures S4 a) and S4 b) represent the real and imaginary parts for Au and S4 c) and S4 d) for Ag. The parameters used are the following:

	$\hbar\omega_p$ (eV)	E_F (eV)	E_g (eV)	$W_{ee}(eV^{-1})$	$\hbar\alpha_0$ (eV)	T (K)	K ($eV^{3/2}$)	$\hbar\gamma$ (eV)
Au	8.5	2.54	2.25	0.3	0.22	295	49	0.05
Ag	9.2	3.99	3.68	0.2	0.18	295	58	0.03

Table S1. Parameters for the intraband and interband transitions in bulk Au and Ag.
$\hbar\omega_p$: volume plasmon energy; E_F: Fermi energy; E_g: conduction band energy, W_{ee}: electron-electron scattering cross section; $\hbar\alpha_0$: interband damping; T: temperature, K: interband oscillator strength; $\hbar\gamma$: Drude damping;

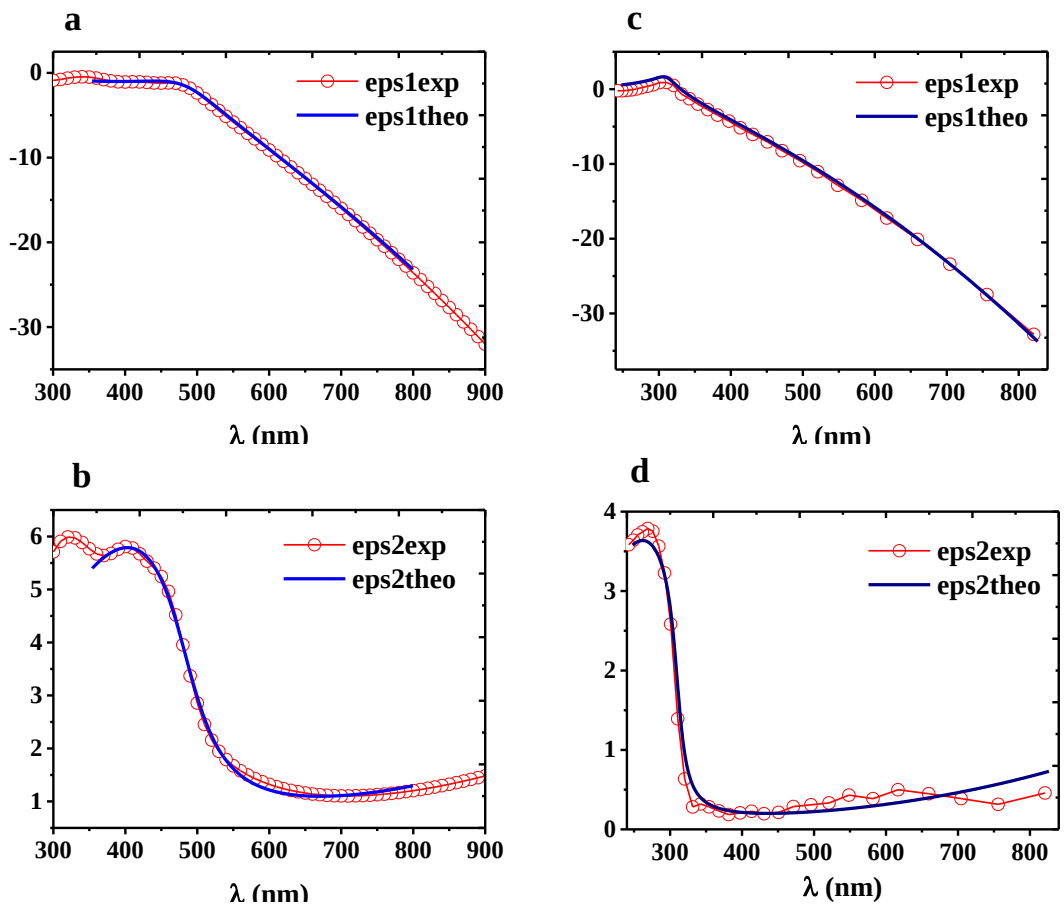

Figure S4. Real and imaginary parts of the bulk dielectric functions. a) and b) for Au and c) and d) for Ag.

b) Optical response of isolated nanoparticles

Second we model the absorption spectrum of the nanoparticles and fit their corresponding experimental spectra. The simple case of isolated nanoparticles in suspension is made using the Maxwell Garnett (MG) model[12]. The effective dielectric function $\tilde{\varepsilon}_{MG}$ is given by :

$$\frac{\tilde{\varepsilon}_{MG}-\tilde{\varepsilon}_0}{\tilde{\varepsilon}_{MG}+(n-1)\tilde{\varepsilon}_0}=f\frac{\tilde{\varepsilon}-\tilde{\varepsilon}_0}{\tilde{\varepsilon}+(n-1)\tilde{\varepsilon}_0}\quad;\ \tilde{\varepsilon}=\tilde{\varepsilon}_f+\tilde{\varepsilon}_{ib} \tag{S4}$$

The absorbance A_i for the various models (i) reported here (MG, BRUG, BRUG-MG or image induced dipole) is given by:

$$A_i=\frac{4\pi}{\lambda}\sqrt{\frac{1}{2}\left[\sqrt{(\Re\varepsilon_i)^2+(\Im\varepsilon_i)^2}-\Re\varepsilon_i\right]}\quad i=MG;\ BRUG;\ BRUG\text{-}MG;\ \| \tag{S5}$$

Where n is the dimensionality of the system ($n = 3$ for the NP in suspension), f is the filling factor of the nanoparticles embedded in the surrounding dielectric with complex dielectric function $\tilde{\varepsilon}_0$, which imaginary part is larger for Ag than for Au NPs because of the UV absorption either of the solvent or substrate in the case of deposited nanoparticles ($\tilde{\varepsilon}_0 = \tilde{n}_0^{\,2}$). $\tilde{\varepsilon}$ is the total dielectric function of the metal (bulk Au or Ag). As shown in the main text, figures 4a) for Au and 4b) for Ag, the fits are quite good for both types of NPs in suspension. The following parameters have been used:

NPs suspension	dimension n	$\hbar\gamma$ (eV)	$\hbar\alpha_0$ (eV)	W_{ee} (eV^{-1})	f	$\Re(\tilde{n}_0)$	$\Im(\tilde{n}_0)$
Au	3	0.06	0.25	0.5	10^{-5}	1.5	$3x10^{-5}$
Ag	3	0.28	0.4	0.3	10^{-5}	1.5	$3x10^{-5}$

Table S2. Parameters used for the Au and Ag nanoparticles in suspension. n : dimension of the system; $\hbar\gamma$: Drude damping; $\hbar\alpha_0$: interband damping constant; W_{ee}: electron-electron scattering cross section ; f : filling factor ; $\Re(\tilde{n}_0)$ (resp. $\Im(\tilde{n}_0)$) real and imaginary part of surrounding medium refractive index.

This Maxwell Garnett model, similar to the well-known Clausius Mosotti relation, is valid for diluted spheres and is exact in the limit of small filling factor f [13]. Short range effects due to the surrounding are privileged via the microscopic local field $E_{loc} = \langle E \rangle + 4\pi \langle P \rangle / 3$, where $\langle E \rangle$ and $\langle P \rangle$ are the average macroscopic electric field and polarization. In addition, for the sizes of NPs considered here (d > 10 nm), one can safely use the bulk dielectric function $\tilde{\varepsilon}$ of the metal because quantum corrections like the spill-out of the d-electron wave functions[14], which leads to a red-shift of the absorption spectrum, are negligible. Therefore the red shifted SP spectra observed here can only be attributed to due to dipolar effects, described with a classical theory.

1 Y. Sun, S. K. Gray, S. Peng, *Phys. Chem. Chem. Phys.* 2011, **13**, 11814.
2 Y. Yang, Y. Yan, W. Wang, J. Li, *Nanotechnology* 2008, **19**, 175603.
3 J. Park, J. Joo, S. G. Kwon, Y. Jang, T. Hyeon, *Angew. Chem. Int. Ed.* 2007, **46**, 4630.
4 M. Pauly, B. P. Pichon, , P.-A. Albouy, S. Fleutot, C. Leuvrey, M.Trassin, J.-L. Gallani, S.Begin-Colin, *J. Mater. Chem.* 2011, **21**, 16018.
5 S. Fleutot, G. L. Nealon, M. Pauly, B. P. Pichon, C. Leuvrey, M. Drillon, J.-L. Gallani, D. Guillon, B. Donnio, S. Begin-Colin, *Nanoscale* 2013, **5**, 1507.
6 J. Lindhard , *Dann. Mat. Pys. Medd.* 1954, **28**, 1.
7 D. Pines, P. Nozières, *The Theory of Quantum Liquids.* 1966, *Vol. 1* (W. A. Benjamin, Inc., New York).
8 J.-Y. Bigot, J.-C. Merle, O. Cregut, A. Daunois, *Phys. Rev. Lett.* 1995, **75**, 4702.
9 J.-Y.Bigot, V. Halté, J.-C. Merle, A. Daunois, *Chem. Phys.* 2000, **251**, 181.
10 V. Halté, A. Benabbas, A., J.-Y.Bigot. *Optics Express* 2008, **16**, 11611.
11 P.B. Johnson, R. W. Christy, *Phys. Rev.* 1972, **86**, 4370.
12 J. C. M. Garnett, *Philos. Trans. R. Soc. Lond.* 1904, **203**, 385.
13 R Landauer,. *AIP Conference Proceedings* 1978, **40**, 2.

14 J. Lermé, H. Baida, C. Bonnet, M. Broyer, E. Cottancin, A. Crut, P. Maioli, N. Del Fatti, F. Vallée, M. Pellarin *J. Phys. Chem. Lett.* 2010, **1**, 2922.